J Mater Sci (2020) 55:8829–8842

Ceramics

Structural and electrical characterization of hydrothermally deposited piezoelectric $(K,Na)(Nb,Ta)O_3$ thick films

Takahisa Shiraishi[1,*], Yuta Muto[2], Yoshiharu Ito[3], Takanori Kiguchi[1], Kazuhisa Sato[4,5], Masahiko Nishijima[6], Hidehiro Yasuda[4,5], Hiroshi Funakubo[3], and Toyohiko J. Konno[1]

[1] *Institute for Materials Research, Tohoku University, Sendai 980-8577, Japan*
[2] *School of Engineering, Tohoku University, Sendai 980-8577, Japan*
[3] *School of Materials and Chemical Technology, Tokyo Institute of Technology, Yokohama 226-8502, Japan*
[4] *Research Center for Ultra-High Voltage Electron Microscopy, Osaka University, Osaka 567-0047, Japan*
[5] *Division of Materials and Manufacturing Science, Graduate School of Engineering, Osaka University, Osaka 565-0871, Japan*
[6] *The Electron Microscopy Center, Tohoku University, Sendai 980-8577, Japan*

Received: 18 December 2019
Accepted: 7 April 2020
Published online: 22 April 2020

ABSTRACT

$(K_{0.89}Na_{0.11})(Nb_{0.85}Ta_{0.15})O_3$ thick films were epitaxially grown at 200 °C on (001)La:$SrTiO_3$ and (001)$_c$$SrRuO_3$//(001)$SrTiO_3$ substrates by hydrothermal method, and their crystal structures and electrical properties were investigated. Film thickness increased with deposition time and reached 6 μm in 10 h. High-temperature X-ray diffraction measurement showed that successive phase transitions from orthorhombic to tetragonal and from tetragonal to cubic phases take place at 120 and 400 °C, respectively. Microstructure analyses were performed by using electron microscopy, which revealed the existence of two types of stripe patterns with a width of 100 nm or less. In addition, scanning transmission electron microscopy–energy-dispersive X-ray spectroscopy elemental mapping showed that Nb/(Nb + Ta) ratio of the deposited films abruptly changed around 700 nm in thickness. Annealing at 500 °C led to the reduction in leakage current density from 10^2 to 10^{-5} A/cm^2 at 30 kV/cm, showing that annealing is an effective way to improve insulation. Relative dielectric constant (ε_r) decreased linearly with increasing frequency, reaching 450 at 10 kHz. Polarization–electric field hysteresis loop and field-induced stain curve were measured by piezoelectric force microscopy, which showed remanent polarization (P_r) of 30 μC/cm^2 and piezoelectric constant ($d_{33,PFM}$) of 70 pm/V. These results demonstrate that $(K,Na)(Nb,Ta)O_3$ thick films with superior electrical properties can be fabricated by the low-temperature deposition technique.

Address correspondence to E-mail: takahisa.shiraishi@imr.tohoku.ac.jp

https://doi.org/10.1007/s10853-020-04663-x

Introduction

In view of growing interests in new technologies, such as Internet of Things (IoT) networks, the realization of various devices (e.g., sensors, actuators, and energy-harvesters) with high-performance piezoelectric films become essential [1–4]. $Pb(Zr,Ti)O_3$-based materials are most widely used in piezoelectric devices owing to their superior piezoelectricity near morphotropic phase boundary between the rhombohedral and tetragonal phases [5]. However, there are concerns over harmful effects in the use of lead-containing materials in the environment and human body. Therefore, it is desirable to establish lead-free materials with piezoelectric properties comparable to $Pb(Zr,Ti)O_3$-based family [6, 7]. In addition, piezoelectric films exceeding 1 μm thickness are required for sensors and actuators [8, 9].

In this regard, $(K,Na)NbO_3$, which is lead-free, has excellent piezoelectric properties in the vicinity of polymorphic phase boundaries between the orthorhombic and tetragonal phases [10]. This phase boundary exists at 210 °C in pure $(K,Na)NbO_3$ [11, 12], but can be adjusted to around room temperature by compositional modification [10, 13, 14]. For example, Saito et al. [15] reported that $(K,Na,Li)(Nb,Ta,Sb)O_3$ with polymorphic phase boundary near room temperature exhibits groundbreaking piezoelectric properties. It was also demonstrated that $(K,Na)NbO_3$ family containing multi-components, such as $(K,Na)(Nb,Sb)O_3$-$(Bi,Na)ZrO_3$, forms new phase boundaries composed of rhombohedral and tetragonal phases [16]. Thus, the piezoelectric properties of $(K,Na)NbO_3$-based materials are comparable with those of $Pb(Zr,Ti)O_3$-based materials, and have attracted much attention as a promising candidate as a lead-free piezoelectric material.

Although compositional modification of $(K,Na)NbO_3$ is an effective technique to tune polymorphic phase boundaries and improve piezoelectric properties, deposition of high-quality stoichiometric $(K,Na)NbO_3$-based films has always been a challenge due to the high volatility of K and Na [17, 18]. In this respect, the hydrothermal method is one of the solutions to that challenge. This method is a wet process with alkaline solution and presently used to fabricate various functional materials [19–24]. An important characteristic of this method is that it is a process working at a low temperature: Previous reports showed that $(K,Na)NbO_3$films can be obtained between 100 and 240 °C [25–27]. These process temperatures are much lower than those of commonly employed deposition methods, such as sputtering [28], sol–gel [29], or pulsed laser deposition [30], suggesting that K and Na elements do not volatilize. Another important characteristic of the hydrothermal method is the controllability of film thickness over a wide range. Since the deposition rate strongly depends on the parameters, such as concentration and temperature [25, 31], the film thickness can be adjusted to several hundred nanometers to several ten micrometers, thereby making the hydrothermal method as an attractive way to produce $(K,Na)NbO_3$-based thick (1–100 μm) films [32, 33].

In addition, it is known that of Nb-site in $(K,Na)NbO_3$ plays an important role in controlling phase transition temperatures [10]. For example, as the content of Ta which substitutes Nb increases, the orthorhombic–tetragonal phase transition temperature decreases [34]. In fact, we reported that $(K,Na)(Nb,Ta)O_3$ films with controlled composition can be obtained by a hydrothermal method [35]. Handoko et al. also reported the hydrothermal deposition of $(K,Na)NbO_3$ films, where Nb atom was substituted with Li and Ta [36]. However, there are few reports on the electrical properties of hydrothermally deposited $(K,Na)NbO_3$-based films.

In this work, we chose Ta to substitute Nb and investigated the crystal structures, microstructures, and electrical properties of hydrothermally deposited $(K,Na)(Nb,Ta)O_3$ thick films.

Materials and methods

$(K_{0.89}Na_{0.11})(Nb_{0.85}Ta_{0.15})O_3$(KNNT) films were deposited on (001)La:$SrTiO_3$ and (001)$_c$$SrRuO_3$//(001)$SrTiO_3$ substrates by the hydrothermal method. For the latter, 50 nm-thick $SrRuO_3$ layers were epitaxially grown as bottom electrodes by radio frequency magnetron sputtering. Potassium hydroxide (86.0%, KANTO CHEMICAL CO., INC) and sodium hydroxide (97.0%, KANTO CHEMICAL CO., INC) were first dissolved in ion-exchanged water with a concentration of 7 mol/dm^3. Then, Nb_2O_5 and Ta_2O_5 powders (99.95%, KANTO CHEMICAL CO., INC) with 0.0012 mol in total were put into 20 mL of the solution, where the aforementioned substrates were

immersed, and finally they were sealed in autoclaves. In order to achieve high deposition rates, [KOH]/([KOH] + [NaOH]) and $[Ta_2O_5]/([Ta_2O_5] + [Nb_2O_5])$ ratios were adjusted to 0.9 and 0.2, respectively [27, 35]. The autoclaves were heated in an oven at 200 °C for 1.5–10 h. The deposited films were taken out after cooling, washed ultrasonically in ion-exchanged water, ethanol, and acetone, and then dried at 150 °C for 1 h in air.

Average film composition was determined by X-ray fluorescence spectroscopy (XRF, PW4400, PANalytical). K/(K + Na) and Ta/(Ta + Nb) ratios were estimated by the fundamental parameter method calibrated with $KNbO_3$, $NaNbO_3$, and $KTaO_3$ films. Film thickness and surface morphology were evaluated by using scanning electron microscopy (SEM, HITACH S-4800). Crystal structure was investigated by X-ray diffractometry (XRD, Philips X'Pert MRD system). In this report, crystallographic orientation will be indicated by using pseudo-cubic indices, and denoted as $\{hkl\}_c$. To investigate phase transition temperatures, high-temperature XRD measurement was carried out using XRD equipment with a temperature-controllable stage (Anton Paar DHS1100). Microstructure observations were performed by using transmission electron microscopy (TEM, Hitachi H-3000 operating at 2 MV) and scanning-TEM (STEM, JEOL JEM-ARM200F Cold FEG operating at 200 kV and Thermo Fisher Scientific Titan^3 60–300 equipped with probe-corrector operating at 300 kV). The ultra-high voltage electron microscope (UHVEM) operating above 1 MV enables microstructure analyses even in a thick specimen in the observation direction thanks to its high transmission power [37], which is suitable for observing threading dislocations. Samples for TEM specimens were prepared using mechanical polishing followed by Ar ion milling. Selected area electron diffraction (SAED) patterns of the deposited films were obtained using an aperture with 750 nm in diameter after adjusting the zone axis to $[010]_{STO}$. The conditions for STEM observation are: Zone axis was set to $[010]_{STO}$, convergence semi-angle (α) was set to 20 mrad, and acceptance semi-angles, β_{in}–β_{out}, were set to 90–175 and 40 – 160 mrad for high-angle annular dark (HAADF) and low-angle annular dark field (LAADF)–STEM images, respectively. Elemental mappings were obtained by STEM–energy-dispersive X-ray spectroscopy (STEM–EDS, JED-2300 T) using K-*K*, Na–*K*, Nb-*K*, and Ta-*L* characteristic X-rays.

To measure electrical properties, Pt top electrodes of 100 μm in diameter were deposited at room temperature on KNNT//$(001)_c$$SrRuO_3$//$(001)SrTiO_3$ by Ar-ion beam sputtering, forming a capacitor structure. Pt/KNNT/$SrRuO_3$ capacitor was then annealed at 200–500 °C for 10 min in O_2 atmosphere. Leakage current density and dielectric constant were measured using an electrometer (KEITHLEY6517B) and a precision LCR meter (Agilent E4980), respectively. Ferroelectric and piezoelectric properties were measured by piezoelectric force microscopy (PFM; SII SPA400).

Results

Crystal structures

Figure 1a shows film thickness as a function of deposition time, t, for KNNT films on (001)La:$SrTiO_3$ substrates. In this study, $t = 0$ is defined as the time when the autoclave is placed in the bath. Thus, the observed film thickness was nearly zero up to 1 h because temperature in the autoclave did not reach a temperature for hydrothermal reaction to occur. As seen, the film thickness started to increase at 1.5 h, and reached 6 μm in 10 h. Figure 1b shows XRD $2\theta - \omega$ patterns for the films as a function of deposition time. In all the patterns, only $\{00l\}_c$ peaks (l = integer) originating from the oxide films were observed, suggesting that the deposited films have an epitaxial orientation relationship with the substrates, and grown as a perovskite single phase. A close examination on the peaks due to the KNNT films reveals the peaks were asymmetrical, i.e., exhibit non-negligible intensities in the high 2θ angle sides. This indicates the formation of domains with $0k0_c$ and $00l_c$ orientations. The XRD ϕ-scan pattern shown in Fig. 1c was measured at 2θ corresponding to the peak arising from $(011)_c$ plane of the KNNT film obtained at $t = 10$ h. The observed fourfold symmetric peaks confirmed that the deposited film was epitaxially grown with $\{001\}_c$-orientation on substrate. Figure 1d shows the deposition time dependence of out-of-plane lattice constant for KNNT films. As mentioned above, diffraction peaks of KNNT can be assigned to $0k0$ and $00l_c$. However, it is difficult to separate these peaks because the lattice constants are so close. Therefore, the lattice constant was estimated from 2θ position of the peak top. As seen, the lattice

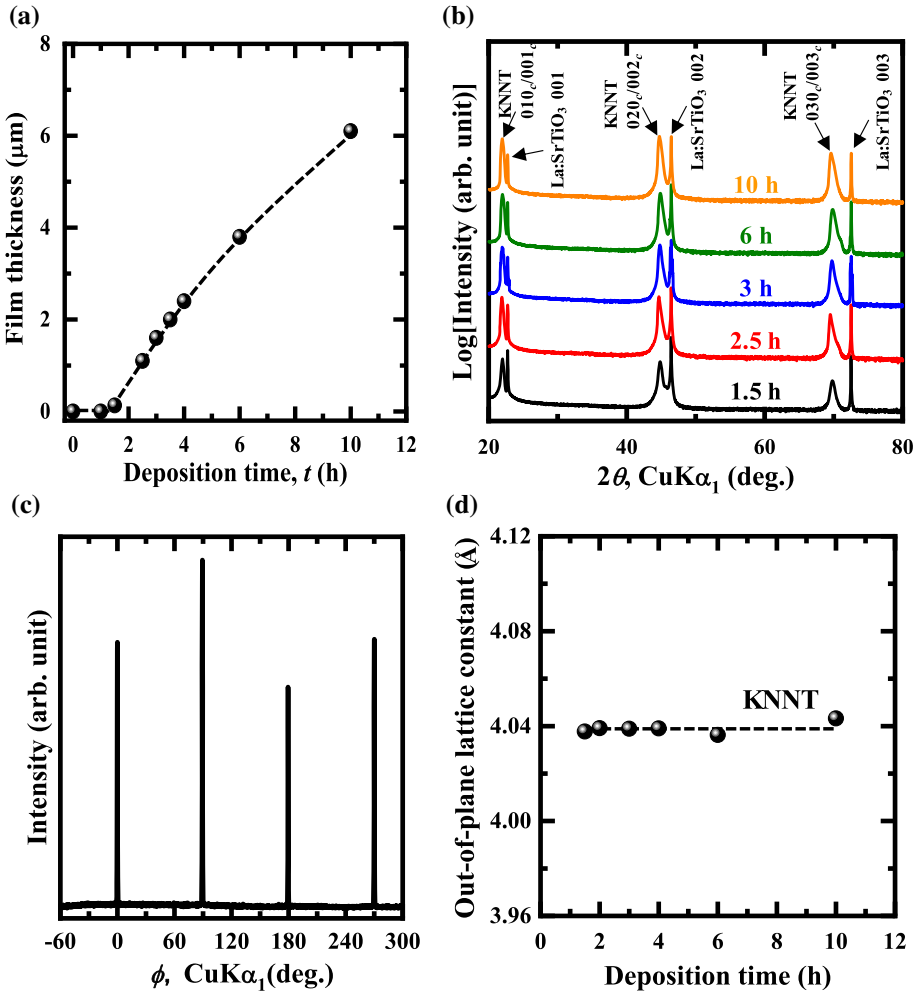

Figure 1 **a** Film thickness as a function of deposition time. **b** XRD $2\theta - \omega$ patterns for the KNNT films deposited on (001)La:$SrTiO_3$ substrates with different deposition times. **c** ϕ scan pattern measured for the pseudocubic 011 diffraction peaks of the film prepared in 10 h. **d** Out-of-plane lattice constants of the films as a function of deposition time.

constant was approximately 4.04 Å regardless of deposition time, suggesting that the film is compositionally uniform across the film thickness.

Figure 2a shows the XRD $2\theta - \omega$ patterns measured at various temperatures for the KNNT film obtained at t = 4 h. As seen, with increasing temperature, a prominent peak, labeled P1, shifts toward the low-angle side up to around 240 °C, and then moves back toward the high-angle side. Careful examination also reveals that a weak peak, labeled P2, emerges at 120 °C, and shifts to the low-angle side until it merges into P1 at about 400 °C. These observations indicate that phase transitions in KNNT have occurred twice. In Fig. 2b, we plot the temperature dependence of out-of-plane lattice constants for the KNNT films, together with that of La:$SrTiO_3$ substrate, estimated from the patterns in Fig. 2a. This figure shows that the orthorhombic–tetragonal phase transition temperature (T_{O-T}) and the tetragonal–cubic phase transition temperature (T_c: Curie temperature) are 120 and 400 °C, respectively. According to the phase diagram of (K,Na)NbO_3, T_{O-T} and T_c are about 210 and 400 °C [38], whereas T_c of the hydrothermally deposited $(K_{0.88}Na_{0.12})NbO_3$ film was reported to be 450 °C [39]. These observations hence suggest that these phase transition temperatures decreased by Ta substitution. Figure 2c summarizes phase transition temperatures, deduced by the high-temperature XRD study, as a function of film composition, Ta/(Ta + Nb) ratio. The phase transition temperatures decreased with increasing Ta/(Ta + Nb), in particular, the orthorhombic–tetragonal phase boundary has dropped to 70 °C at Ta/(Ta + Nb) = 0.3. This result was similar to the relationship between Ta/(Ta + Nb) ratio and phase transition temperatures reported for (K,Na)(Nb,Ta)O_3 bulk [34]. These observations thus show that the polymorphic phase boundary in the hydrothermally deposited (K,Na)(Nb,Ta)O_3 films can

be adjusted to around room temperature by modifying film composition.

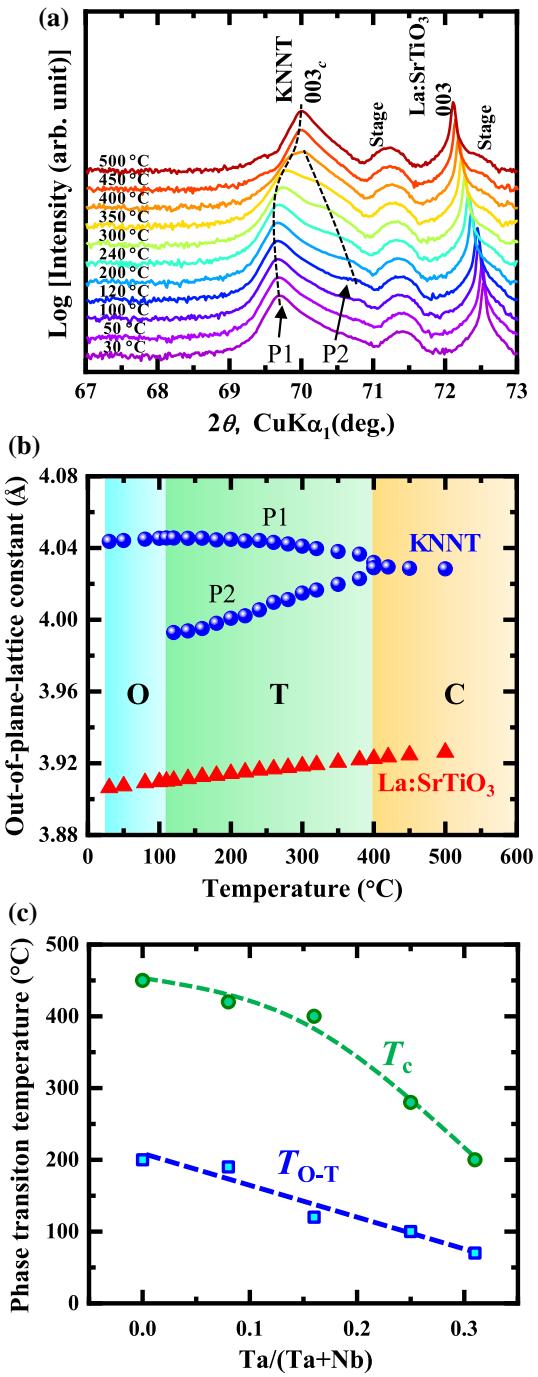

Figure 2 **a** XRD $2\theta - \omega$ patterns measured at various temperatures for the KNNT film deposited at $t = 4$ h on (001)La:$SrTiO_3$ substrates. **b** Out-of-plane lattice constant as a function of temperature. O, T, and C indicate orthorhombic, tetragonal, and cubic phases, respectively. **c** Relationship between film composition, Ta/(Ta + Nb), and phase transition temperatures.

Microstructures

Figure 3a, c shows the plane-view SEM images of KNNT films with different deposition times. As seen, facets (marked by solid lines) were observed in the films deposited at 2.5 and 6 h, indicating that the nuclei generated on surface had grown laterally to form a film. On the other hand, after deposition for 10 h, pits (marked by dashed lines) were observed throughout the surface, and they were formed along the $[100]_{STO}$ and $[010]_{STO}$ directions. It is assumed that surface of these films was etched by alkaline. Ishikawa et al. reported that alkaline solution etches the deposited film from surface and grain boundary

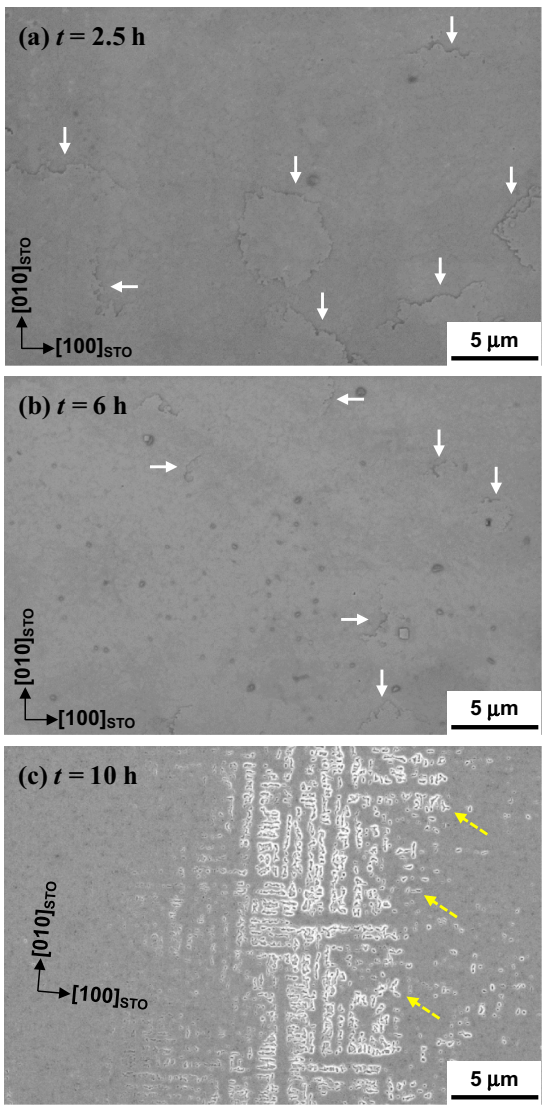

Figure 3 Plane-view SEM images of KNNT films deposited at t = **a** 2.5, **b** 6 and **c** 10 h. Solid and dashed arrows indicate the facets and pits, respectively.

under hydrothermal condition [40, 41]. In addition, it has been reported that grain boundaries formed in epitaxial films are along specific crystal orientation [42]. Therefore, it was found that there was an optimal deposition time for fabricating KNNT thick films.

Figure 4a shows a cross-sectional bright-field TEM image of the KNNT (t = 4 h) film observed by UHVEM, showing a smooth film/substrate interface and a flat surface of the film. Note the presence of diffraction contrasts along the direction perpendicular to the interface, most likely arising from threading dislocations. It should also be noted that a weak diffraction contrast in the horizontal direction was observed at about 700 nm in film thickness indicated by the dashed line, where some of the aforementioned threading dislocations were discontinued or bent. This means that there is a structural boundary within the film, and that KNNT film has a bilayer structure. Figure 4b shows the SAED pattern for KNNT/La:$SrTiO_3$. As seen, the diffraction spots arising from the film and substrate were clearly observed. The estimated in-plane lattice constant of KNNT film was 3.98 Å, which was larger than that of La:$SrTiO_3$ substrate, 3.91 Å. This indicates that the strain caused by lattice mismatch has been relaxed.

In order to investigate a possible bilayer structure in detail, STEM observations were performed for the same film, as shown in Fig. 4. Figure 5a, d shows STEM–EDS mappings obtained using characteristic K-*K*, Na-*K*, Nb-*L*, and Ta-*L* X-rays, respectively. No significant contrast changes have been detected for K and Na in the mapping, whereas the intensities of Nb and Ta discontinuously changed at the thickness. The Ta/(Ta + Nb) ratios of the lower and upper layers were estimated to be 0.17 and 0.13, respectively. Figure 5e shows the intensity profiles for each element obtained from the EDS mappings, showing that all profiles have changed discontinuously around 700 nm in thickness, as indicated by the dashed arrow. These findings led us to conclude that the hydrothermally deposited KNNT thick films have a bilayer structure consisting of a perovskite phase with different Ta/(Ta + Nb) ratios.

Figure 6a shows a LAADF–STEM image from the same region. The interface between lower and upper layers was located around 700 nm in film thickness, but not conceivable in their imaging mode, which is basically a Z-contrast. Figure 6b shows a HAADF–STEM image taken from the rectangular region shown in Fig. 6a, where bright spots correspond to cation positions. As seen here, the lower and upper layers formed a coherent interface, and no local deformations such as misfit and edge dislocations were observed, indicating that the in-plane lattice mismatch between the lower and upper layers is very small.

Figure 7a, b shows cross-sectional HAADF–STEM and bright-field STEM images of a KNNT film deposited at t = 4 h on a $(001)_c SrRuO_3//(001)SrTiO_3$ substrate. The thickness of the deposited film was 3 μm, which was equivalent to that of KNNT film on the $SrTiO_3$ substrate. In addition, the two types of stripe patterns were observed: one shown in Fig. 7a, in the $[101]_{STO}$ and $[-101]_{STO}$ directions, and the other in Fig. 7b at 60 and 120° angle to the film/$SrRuO_3$ interface. In addition, widths of these patterns were less than 100 nm. These results suggest that KNNT film deposited at low temperature has a multidomain structure.

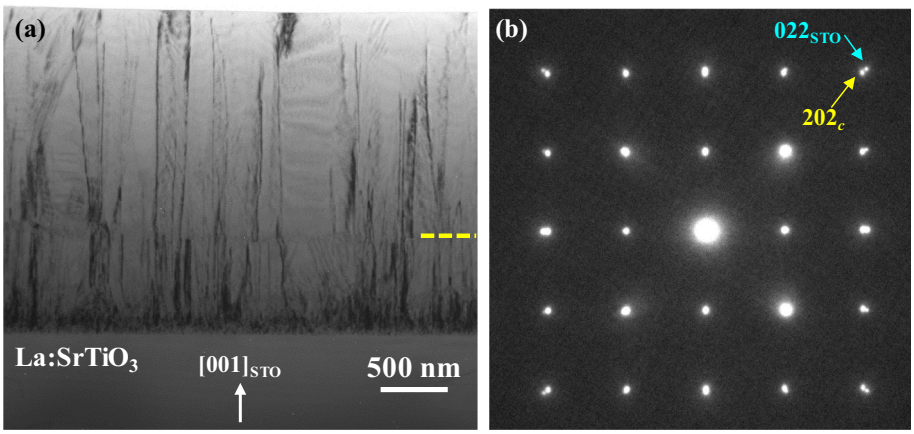

Figure 4 **a** Cross-sectional bright-field TEM image of the KNNT film deposited at t = 4 h on (001)La:$SrTiO_3$ substrates. Note the presence of line contrasts, which arise form dislocations. Dashed line indicates the position at which a diffraction contrast changes. **b** $[010]_c$ zone axis SAED pattern for KNNT/La:$SrTiO_3$.

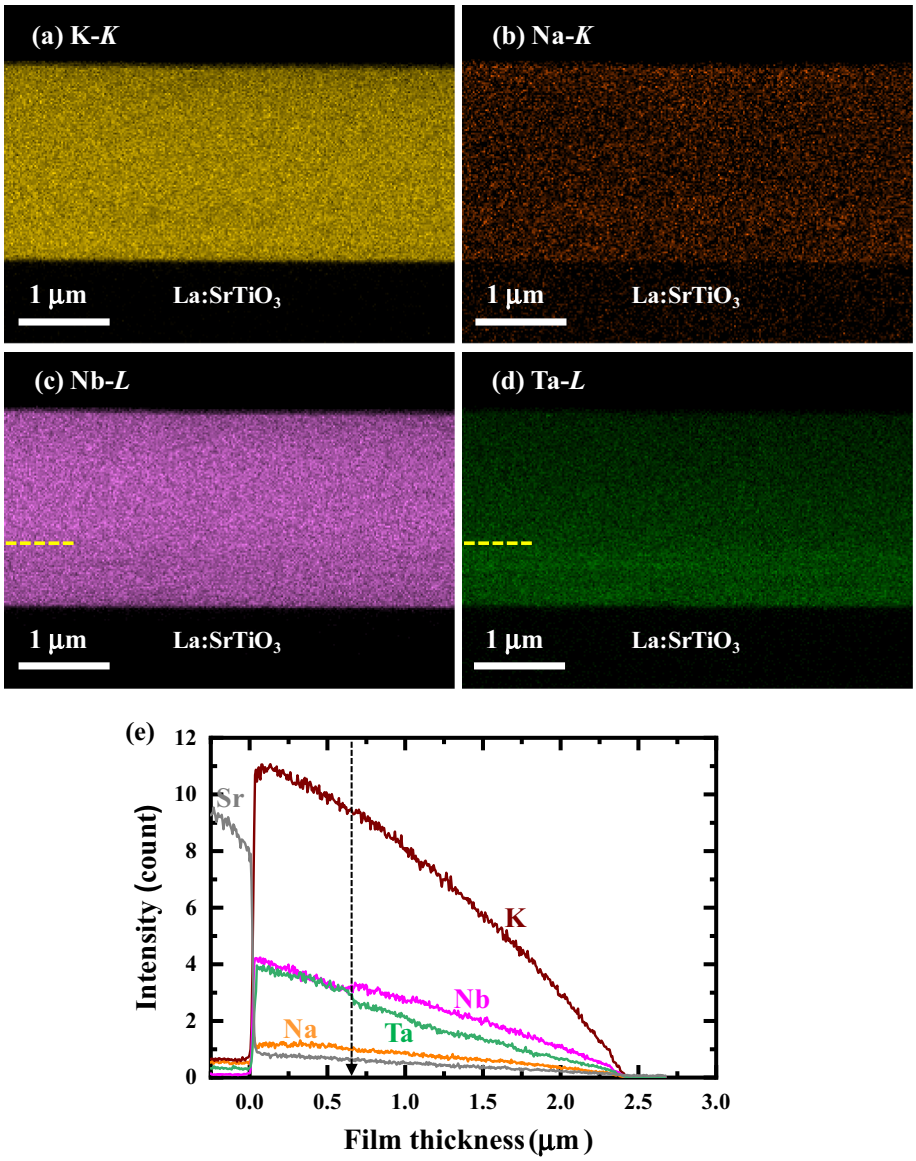

Figure 5 STEM–EDS mappings obtained using **a** K-*K*, **b** Na–*K*, **c** Nb-*L*, and **d** Ta-*L* characteristic X-rays for the same film as shown in Fig. 4. **e** Intensity profiles for each element obtained from EDS mappings. Sr profile indicates the position of substrate. Dashed arrow indicates the position of the abrupt change.

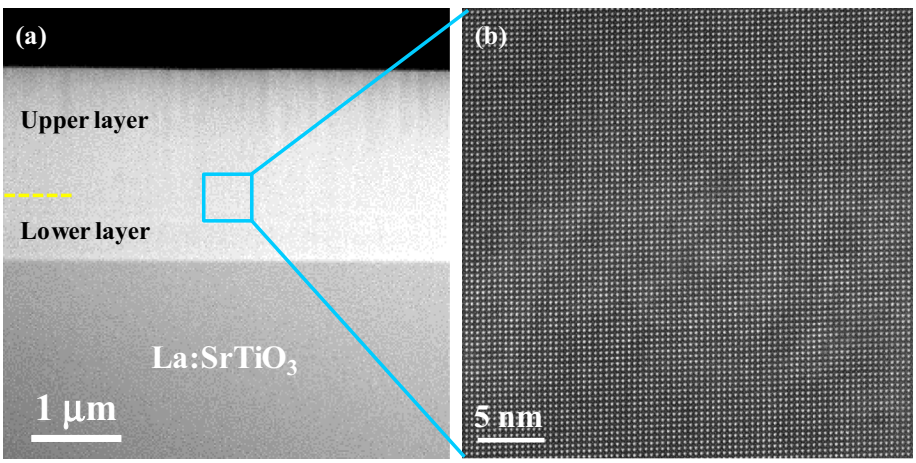

Figure 6 **a** Cross-sectional LAADF–STEM image. Dashed line indicates the interface between layers having different Ta/(Ta + Nb) ratios. **b** HAADF–STEM image of the rectangle region shown in **a**.

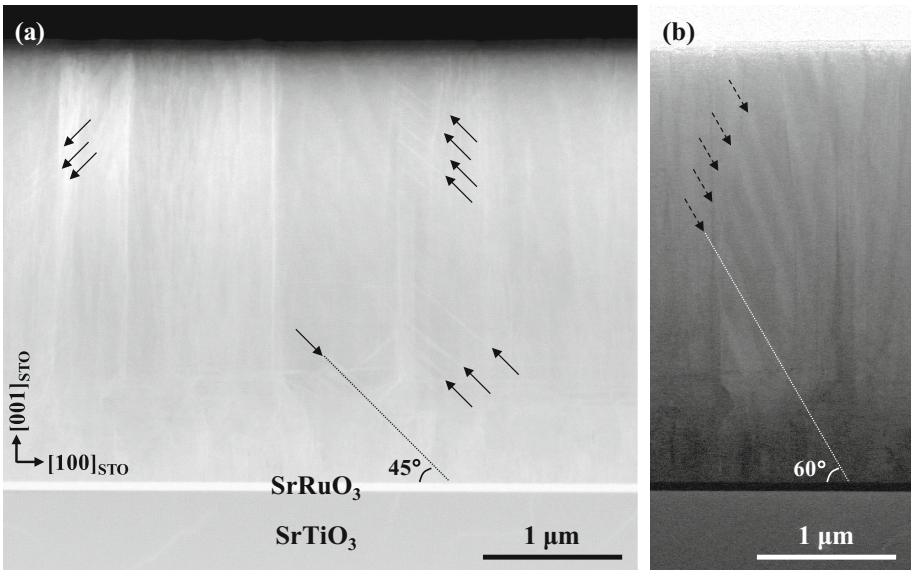

Figure 7 Cross-sectional **a** HAADF–STEM and **b** bright-field STEM images of 3-μm-thick KNNT film deposited on $(001)_c SrRuO_3$// $(001)SrTiO_3$ substrate. Solid and dashed arrows indicate the stripe patterns.

Annealing effect on crystal structures and microstructures

Figure 8a shows annealing temperature dependence of XRD $2\theta - \omega$ patterns measured at room temperature for 3 μm-thick KNNT films deposited on $(001)_c$-$SrRuO_3$//$(001)SrTiO_3$ substrates. In all the patterns, only peaks due to the perovskite phase were observed. Figure 8b shows a SAED pattern observed along the $[010]_c$ zone axis for the KNNT film annealed at 500 °C. The spot pattern confirms that the epitaxial relationship between the film and substrate was maintained before and after the annealing. Figure 8c shows out-of-plane lattice constant estimated from Fig. 8a as a function of annealing temperature. From this result, it was found that the lattice constant slightly decreased for the specimen annealed above 400 °C. This temperature was consistent with T_c obtained by high-temperature XRD measurement, as shown in Fig. 2b. Thus, it is considered that the observed slight change in the lattice constant was caused by change in the crystal structure, accompanying the phase transition. Figure 8d shows microstructure of the KNNT film annealed at 500 °C, showing stripe patterns, confirming that the annealed films also have multidomain structure.

Electrical properties of annealed films

Figure 9a shows leakage current density–electric field (J–E) curves for the as-deposited and annealed films with 3 μm thickness. Leakage current density was reduced to values as low as 10^{-5} A/cm^2 at 30 kV/cm after 500 °C annealing. Practically, this means that high electric field scan be applied after annealing. It is well known the hydrothermally deposited films often contain OH^- and H_2O derived from alkaline source solution, leading to poor insulation [43, 44]. Thus, high-temperature annealing is one of the effective ways to eliminate these impurities. In fact, we have already demonstrated that the desorption of impurities derived from OH^- and H_2O completes by an annealing treatment above 500 °C [45]. Namely, we have reported, using thermal desorption spectroscopy, that the desorption process consisted of two steps [45, 46]. In the first step, H_2O around film surface and grain boundary is removed, decreasing leakage current density. This means that high electric fields can be applied after annealing. In the second step, the desorption of OH^- contained around the film/substrate interface occurs, resulting in improved ferroelectric and piezoelectric properties. Based on these observations, we can suggest here that the leakage current density of KNNT films decreased, as seen in Fig. 9a. Figure 9b shows frequency dependence of relative dielectric constant (ε_r) and dielectric loss (tan δ) of the film annealed at 500 °C. As seen, ε_r decreased with increasing frequency. The value for ε_r at 10 kHz was 450, which is higher than, 430, the reported value for 3-μm-thick $(K_{0.88}Na_{0.12})$-NbO_3 film [47]. This value is one of the consequences of Ta substitution, and a similar tendency has been reported for $(K,Na)(Nb,Ta)O_3$ bulk. On the other hand, tan δ was approximately constant between 10^2

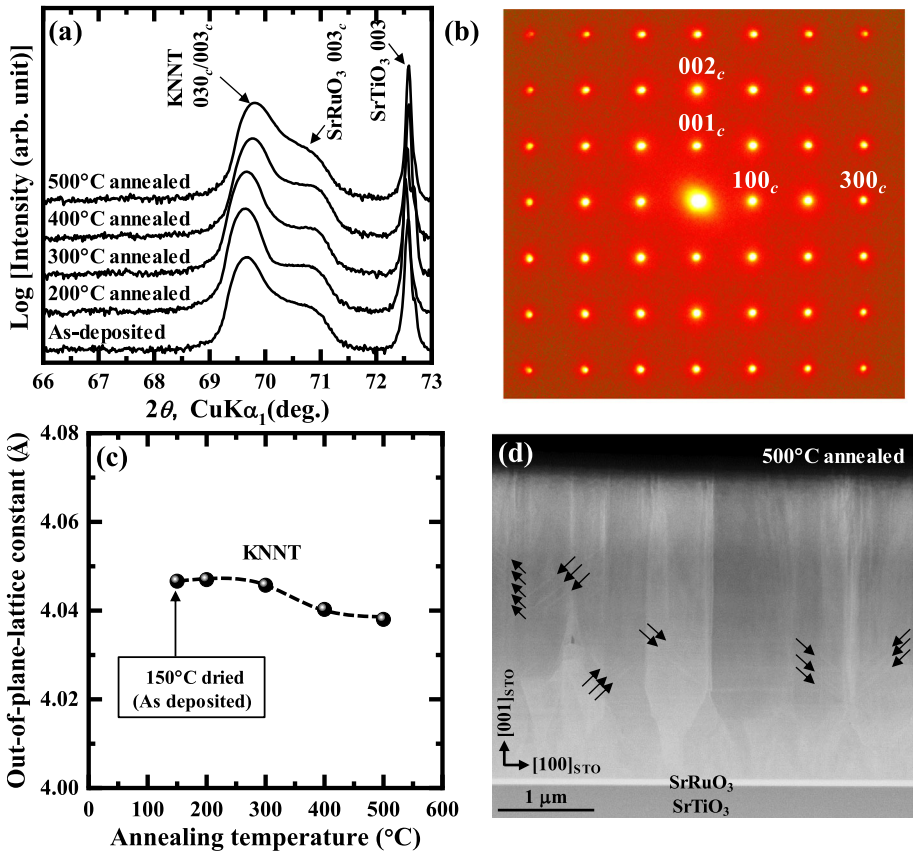

Figure 8 **a** XRD $2\theta - \omega$ patterns for 3-μm thick KNNT films deposited on $(001)_c SrRuO_3//(001)SrTiO_3$ substrates as a function of annealing temperature. **b** $[010]_c$ zone axis SAED pattern of KNNT film annealed at 500 °C. **c** Out-of-plane lattice constants as a function of annealing temperature. **d** Cross-sectional HAADF–STEM image of the KNNT film annealed at 500 °C. Solid arrows indicate the stripe patterns.

and 10^6 Hz. It was thus found that dielectric dispersion occurs above 10^6 Hz.

Figure 10 shows a polarization–electric field (P–E) hysteresis loop and a field-induced strain–electric field (S–E) curve of the film annealed at 500 °C. The observed P–E hysteresis loop already suggests ferroelectricity, with coercive field (E_c) and remanent polarization (P_r) were 60 kV/cm and 30 μC/cm^2, respectively. In addition, the piezoelectric constant ($d_{33,PFM}$) estimated from S–E curve was 70 pm/V, which was higher than the reported values for (K,Na)NbO_3 films deposited by the hydrothermal method [47].

Discussion

Deposition mechanism of KNNT thick film

KNNT films possess a bilayer structure, containing of layers with different Ta/(Ta + Nb) ratio. According to the relationship between the film thickness and deposition time (Fig. 1a), a lower layer with 700 nm thickness was deposited at an early stage in the deposition process. We now discuss a possible nucleation and growth mechanism of the KNNT film. As the autoclave temperature increases, the raw powders, Nb_2O_5 and Ta_2O_5, dissolve in the aqueous solutions of KOH and NaOH in the form of Nb and Ta ions. These cations react with anions formed octahedrally coordinated clusters, which nucleate on the substrate surface. As the deposition proceeds, the nuclei grow laterally to form a film. However, Zhou et al. [48] reported that the dissolution behaviors of Nb_2O_5 and Ta_2O_5 for alkaline solution are actually different. Along the same line, we have previously reported that the synthesis time for the formation of perovskite phase became shorter, as $[Ta_2O_5]/([Ta_2O_5] + [Nb_2O_5])$ ratio in the raw powders increased [35]. These observations strongly suggested that Ta_2O_5 forms a perovskite phase more easily than Nb_2O_5 in hydrothermal conditions. Thus, it is considered that a perovskite phase having a higher Ta/(Ta + Nb) ratio was formed in the early stage of deposition process. In fact, no compositional distribution was observed in $(K_{0.88}Na_{0.12})NbO_3$ thick films deposited by the hydrothermal method.

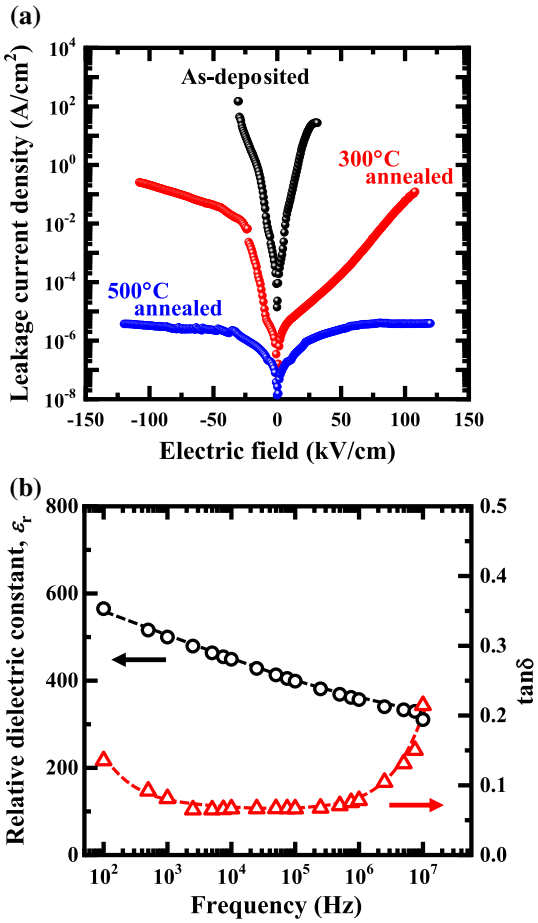

Figure 9 **a** *J–E* curves for a 3-μm-thick KNNT films deposited on $(001)_c SrRuO_3//(001)SrTiO_3$ substrates as a function of annealing temperature. **b** Frequency dependencies of relative dielectric constant (ε_r) and dielectric loss (tan δ) of the film annealed at 500 °C.

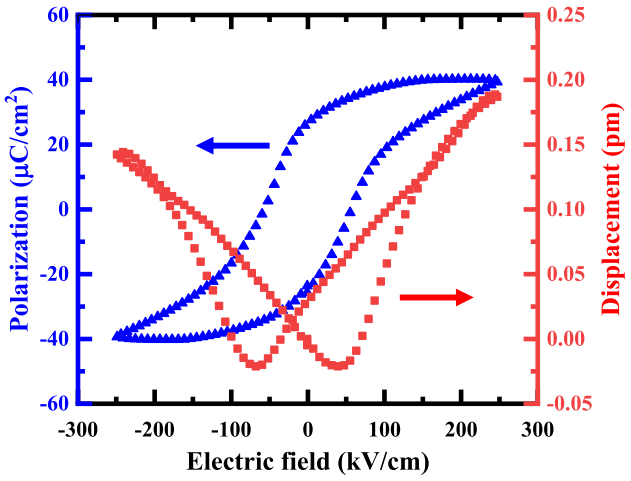

Figure 10 *P–E* hysteresis loop and *S–E* curve of a 3-μm-thick KNNT film annealed at 500 °C.

Improvement in piezoelectricity

It is well known that the fabrication of multilayer structure composed of oxides with different composition is an effective way to improve the electrical properties [49, 50]. In many cases, the difference in composition between the layers is controlled to be large, for example $KNbO_3/KTaO_3$ and $Pb(Zr_{0.52}Ti_{0.48})O_3/Pb(Zr_{0.8}Ti_{0.2})O_3$. According to the EDS mappings for KNNT film, the Ta/(Ta + Nb) ratios of the lower and upper layers were estimated to be 0.17 and 0.13, respectively, indicating that the difference in chemical composition between upper and lower layers was very small. Thus, it can be regarded as a stack structure composed of materials with almost the same chemical composition. In addition, thickness of KNNT was 3 μm, while that of a lower layer was 700 nm. Therefore, it is considered that the effect of bilayer structure on the electrical properties is very small.

Piezoelectric properties heavily depend on the intrinsic and extrinsic responses of the material under electric fields [51]. An intrinsic response is a contribution from the displacements of individual ions, within single domain. On the other hand, an extrinsic response is the one due to domain-wall motions and is observed in a multidomain structure. As shown in Figs. 7 and 8, KNNT films deposited in the present study exhibited stripe patterns. There are two possibilities regarding the origin of these patterns. One is a compositional deviation. It is known that HAADF–STEM image is essentially *Z*-contrast, i.e., its contrast is approximately proportional to Z^2 (Z; average atomic number in an atomic column). However, as shown in Fig. 5, no contrasts variation with a stripe shape was observed. The other possibility is the ferroelectric domains. According to the result of high-temperature XRD measurement (Fig. 2), the crystalline phase of KNNT film assumes the orthorhombic phase at room temperature. Thus, not only 180 and 90° domains but also 60 and 120° domains can be formed. In this case, the domain-wall density is expected to increase, resulting in a high extrinsic response. Therefore, it is considered that stripe patterns represent a multidomain structure of ferroelectric domains, rather than compositional deviation, and leads to the enhanced piezoelectric response of the KNNT film.

In a thick film, thermal strain resulting from differences in the thermal expansion coefficients

between the film and substrate plays an important role in the formation of the domains [52]. According to the previous reports, thermal expansion coefficients of $KNbO_3$, $NaNbO_3$, $KTaO_3$, $(K_{0.5}Na_{0.5})NbO_3$, $K(Ta_{0.63}Nb_{0.37})O_3$, and $SrTiO_3$ are reported to be 4×10^{-6}, 16×10^{-6}, 4×10^{-6}, 8×10^{-6}, 6.6×10^{-6}, and 11×10^{-6}/°C, respectively [53–56], and the thermal strain, $\varepsilon_{thermal}$, can be calculated using the following equation:

$$\varepsilon_{thermal} = (\alpha_{substrate} - \alpha_{film})'(T_d - T_m) \quad (1)$$

where $\alpha_{substrate}$ and α_{film} are the respective thermal expansion coefficient of the substrate and the film, T_d and T_m are the deposition and atmospheric temperature, respectively. From this equation, thermal strain generated in $KNbO_3/SrTiO_3$, $NaNbO_3/SrTiO_3$, $KTaO_3/SrTiO_3$, $(K_{0.5}Na_{0.5})NbO/SrTiO_3$, and $K(Ta_{0.63}Nb_{0.37})O_3/SrTiO_3$ was estimated to be 12×10^{-4}, -9×10^{-4}, 12×10^{-4}, 5×10^{-4}, and 7.4×10^{-4}, respectively. Note that the $NaNbO_3$ film deposited on the $SrTiO_3$ substrate was subject to tensile strain. In the present study, the chemical composition of the deposited film is $(K_{0.89}Na_{0.11})(Nb_{0.85}Ta_{0.15})O_3$. Thus, by taking an arithmetic average, it is considered that a compressive strain was induced to the film. In the case of $\{001\}_c$-oriented epitaxial (K,Na)(Nb,Ta)O_3 films with orthorhombic phase, three types of diffraction peaks, which are assigned to $h00_c$, $0k0_c$, and $00l_c$, can be observed. However, as can be seen from the XRD patterns, only two types of peaks were detected. This suggests that the compressive strain affects the domain structure.

There are many reports on the relationship between film thickness and electrical properties [57–59]. In particular, it is known that piezoelectric constant, d_{33}, improves with film thickness. So far, we have investigated the dielectric and ferroelectric properties of hydrothermally deposited (K,Na)NbO_3 films with different film thickness [27, 32, 47]. As a result, both properties were improved with increasing film thickness. Therefore, it is expected that the piezoelectric property of the hydrothermally deposited KNNT films will be improved as the film thickness increases.

Conclusions

Epitaxial $(K_{0.89}Na_{0.11})(Nb_{0.85}Ta_{0.15})O_3$ films, as thick as 6 μm, were deposited by hydrothermal method. As Ta/(Ta + Nb) ratio increased from 0 to 0.31, the orthorhombic–tetragonal and tetragonal–cubic phase transition temperatures decreased from 200 to 70 °C and from 450 to 200 °C, respectively. STEM–EDS mappings revealed that the deposited thick films possess not a single layer structure but a bilayer structure, where Ta contents exhibited a sudden drop at about 700 nm thickness. In addition, two types of stripe patterns were observed, suggesting the presence of a domain structure. The observed complex domain structure was considered as the effect of Ta substitution. Leakage current density decreased after annealing at 500 °C, and an excellent piezoelectric constant was observed. The present study thus demonstrated that the hydrothermal method is an effective way of depositing high-performance (K,Na)NbO_3-based thick films.

Acknowledgements

This research was partially supported by the Japan Science and Technology Agency (JST) via the Adaptable and Seamless Technology Transfer Program through Target driven R&D (A-STEP) Grant Number JPMJTS1616. In addition, this work was supported by Yashima Environment Technology Foundation. A part of this work was supported by "Advanced Characterization Nanotechnology Platform, Nanotechnology Platform Program of the Ministry of Education, Culture, Sports, Science and Technology (MEXT), Japan" at the Research Center for Ultra-High Voltage Electron Microscopy (Nanotechnology Open Facilities) in Osaka University (Project number: A-17-OS-0042).

Compliance with ethical standards

Conflict of interest The authors declare that they have no conflict of interest.

References

[1] Maenaka K (2016) Sensors in network (5)—future sensor systems in internet of things or trillion sensor universe—. Sens Mater 28:1247–1254

[2] Jeong CK, Han JH, Palneedi H et al (2017) Comprehensive biocompatibility of nontoxic and high-output flexible energy harvester using lead-free piezoceramic thin film. APL Mater 5:074102

[3] Won SS, Seo H, Kawahara M et al (2019) Flexible vibrational energy harvesting devices using strain-engineered-perovskite piezoelectric thin films. Nano Energy 55:182–192

[4] Kanno I (2018) Piezoelectric MEMS: ferroelectric thin films for MEMS applications. Jpn J Appl Phys 57:040101

[5] Panda PK, Sahoo B (2015) PZT to lead free Piezo ceramics: a review. Ferroelectrics 474:128–143

[6] Shrout TR, Zhang SJ (2007) Lead-free piezoelectric ceramics: alternatives for PZT? J Electroceram 19:111–124

[7] Zheng T, Wu J, Xiao D, Zhu J (2018) Recent development in lead-free perovskite piezoelectric bulk materials. Prog Mater Sci 98:552–624

[8] Hindrichsen CG, Møller RL, Hansen K, Thomsen EV (2010) Advantages of PZT thickfilm for MEMS sensors. Sens Actuat A Phys 163:9–14

[9] Fujii E, Takayama R, Nomura K et al (2007) Preparation of (001)-oriented Pb(Zr, Ti)$_O$3 thin films and their piezoelectric applications. IEEE Trans Ultrason Ferroelectr Freq Control 54:2431–2437

[10] Wu J, Xiao D, Zhu J (2015) Potassium−sodium niobate lead-free piezoelectric materials: past, present, and future of phase boundaries. Chem Rev 115:2559–2595

[11] Baker DW, Thomas PA, Zhang N, Glazer M (2009) Structural study of $K_xNa_{1-x}NbO_3$ (KNN) for compositions in the range x = 0.24–0.36. Acta Cryst B 65:22–28

[12] Ishizawa N, Wang J, Sakakura T, Inagaki Y, Kakimoto K (2010) Structural evolution of $Na_{0.5}K_{0.5}NbO_3$ at high temperatures. J Solid State Chem 183:2731–2738

[13] Li JF, Wang K, Zhu FY, Cheng LQ, Yao FZ (2013) (K, Na)NbO_3-based lead-free piezoceramics: fundamental aspects, processing technologies, and remaining challenges. J Am Ceram Soc 96:3677–3696

[14] Zhang Y, Li JF (2019) Review of chemical modification on potassium sodium niobate lead-free piezoelectrics. J Mater Chem C 7:4284–4303

[15] Saito Y, Takao H, Tani T, Nonoyama T, Takatori K, Homma T, Nagaya T, Nakamura M (2004) Lead-free piezoceramics. Nature 432:84–87

[16] Xing J, Zheng T, Wu J, Xiao D, Zhu J (2018) Progress on the doping and phase boundary design of potassium–sodium niobate lead-free ceramics. J Adv Dielectr 8:1830003

[17] Flückiger U, Arend H (1978) On the preparation of pure, doped and reduced $KNbO_3$ single crystals. J Cryst Growth 43:406–416

[18] Hicks WT (1963) Evaluation of vapor-pressure data for mercury, lithium, sodium, and potassium. J Chem Phys 38:1873–1880

[19] Athayde DD, Souza DF, Silva AMA, Vasconcelos D, Nunes EHM, Costa JCD, Vasconcelos WL (2016) Review of perovskite ceramic synthesis and membrane preparation methods. Ceram Int 42:6555–6571

[20] Huang A, Handoko AD, Goh GKL, Pallathadka PK, Shannigrahi S (2010) Hydrothermal synthesis of (00l) epitaxial $BiFeO_3$ films on $SrTiO_3$ substrate. CrystEngComm 12:3806–3814

[21] Morita T, Wagatsuma Y, Morioka H, Funakubo H, Setter N, Cho Y (2004) Ferroelectric property of an epitaxial PZT thin film deposited by a hydrothermal method. J Mater Res 19:1862–1868

[22] Wang D, Yang JO, Guo W, Yang X, Zhu B (2017) Novel fabrication of PZT thick films by an oil-bath based hydrothermal method. Ceram Int 43:9573–9576

[23] Li L, Miao L, Zhang Z, Pu X, Feng Q, Yanagisawa K, Fan Y, Fan M, Wen P, Hu D (2019) Recent progress in piezoelectric thin film fabrication via the solvothermal process. J Mater Chem A 7:16046–16067

[24] Tu S, Ming F, Zhang J, Zhang X, Alshareef HN (2019) MXene-derived ferroelectric crystals. Adv Mater 31:1806860

[25] Shiraishi T, Kaneko N, Ishikawa M, Kurosawa M, Uchida H, Funakubo H (2014) Ferroelectric and piezoelectric properties of $KNbO_3$ films deposited on flexible organic substrate by hydrothermal method. Jpn J Appl Phys 53:09PA10

[26] Kaneko N, Shiraishi T, Kurosawa M, Shimizu T, Funakubo H (2014) Low temperature preparation of $KNbO_3$ films by hydrothermal method and their characterization. Mater Res Symp Proc 1659:49–54

[27] Shiraishi T, Einishi H, Yasui S et al (2011) Growth of epitaxial {100}-oriented $KNbO_3$–$NaNbO_3$ solid solution films on (100)$_c$$SrRuO_3$//(100)$SrTiO_3$ by hydrothermal method and their characterization. Jpn J Appl Phys 50:09ND11

[28] Shibata K, Oka F, Ohishi A, Mishima T, Kanno I (2008) Piezoelectric properties of (K, Na)Nb$_O$3 films deposited by RF magnetron sputtering. Appl Phys Express 1:011501

[29] Yu Q, Li JF, Sun W, Zhou Z, Xu Y, Xie ZK, Lai FP, Wang QM (2013) Electrical properties of $K_{0.5}Na_{0.5}NbO_3$ thin films grown on Nb:$SrTiO_3$ single-crystalline substrates with different crystallographic orientations. J Appl Phys 113:024101

[30] Nguyen MD, Dekkers M, Houwman EP, Vu HT, Vu HN, Rijnders G (2016) Lead-free $(K_{0.5}Na_{0.5})NbO_3$ thin films by pulsed laser deposition driving MEMS-based piezoelectric cantilevers. Mater Lett 164:413–416

[31] Tateyama A, Ito Y, Nakamura Y et al (2019) Effects of starting materials on the deposition behavior of

hydrothermally synthesized {100}$_c$-oriented epitaxial (K, Na)Nb$_O$3 thick films and their ferroelectric and piezoelectric properties. J Cryst Growth 511:1–7

[32] Shiraishi T, Ito Y, Ishikawa M, Uchida H, Kiguchi T, Kurosawa MK, Funakubo H, Konno TJ (2018) Preparation of {001}$_c$-oriented epitaxial (K, Na)NbO_3 thick films by repeated hydrothermal deposition technique. J Ceram Soc Jpn 126:281–285

[33] Shiraishi T, Muto Y, Ito Y, Tateyama A, Uchida H, Kiguchi T, Kurosawa MK, Funakubo H, Konno TJ (2019) Low-temperature deposition of Li substituted (K, Na)Nb$_O$3 films by a hydrothermal method and their structural and ferroelectric properties. J Ceram Soc Jpn 127:388–393

[34] Sung YS, Lee JH, Kim SW et al (2012) Enhanced piezoelectric properties of $(Na_{0.53}K_{0.47})(Nb_{1-x}Ta_x)O_3$ ceramics by Ta substitution. Ceram Int 38S:S301–S304

[35] Muto Y, Shiraishi T, Ito Y, Tateyama A, Uchida H, Kiguchi T, Funakubo H, Konno TJ (2019) Effect of Ta-substitution on the deposition of (K, Na)(Nb, Ta)O3 films by hydrothermal method. Jpn J Appl Phys 58:SLLB12

[36] Handoko AD, Goh GKL (2013) Hydrothermal growth of piezoelectrically active leadfree (Na, K)Nb$_O$3–LiTa$_O$3 thin films. CrystEngComm 15:672–678

[37] Fujita H, Tabata T, Yoshida K, Sumida N, Katagiri S (1972) Some applications of an ultra-high voltage electron microscope on materials science. Jpn J Appl Phys 11:1522–1536

[38] Baker DW, Thomas PA, Zhang N, Glazer AM (2009) A comprehensive study of the phase diagram of K_xNa_{1-x}-NbO_3. Appl Phys Lett 95:091903

[39] Shiraishi T, Kaneko N, Einishi H et al (2013) Crystal structure analysis of hydrothermally synthesized epitaxial $(K_xNa_{1-x})NbO_3$ films. Jpn J Appl Phys 52:09KA11

[40] Ishikawa M, Yazawa K, Fujisawa T, Yasui S, Yamada T, Hasegawa T, Morita T, Kurosawa M, Funakubo H (2009) Growth of epitaxial $KNbO_3$ thick films by hydrothermal method and their characterization. Jpn J Appl Phys 48:09KA14

[41] Ishikawa M, Einishi H, Nakajima M, Hasegawa T, Morita T, Kurosawa M, Saijo Y, Kurosawa M, Funakubo H (2010) Effect of deposition time on film thickness and their properties for hydrothermally-grown epitaxial $KNbO_3$ thick films. Jpn J Appl Phys 49:07HF01

[42] Ito Y, Tateyama A, Nakamura Y, Shimizu T, Kurosawa M, Uchida H, Shiraishi T, Kiguchi T, Konno TJ, Ishikawa M, Funakubo H (2019) Growth of epitaxial (K, Na)NbO_3 films with various orientations by hydrothermal method and their properties. Jpn J Appl Phys 58:SLLB4

[43] Chien AT, Xu X, Kim JH, Sachleben J, Speck JS, Lange FF (1999) Electrical characterization of $BaTiO_3$ heteroepitaxial thin films by hydrothermal synthesis. J Mater Res 14:3330–3339

[44] Handoko AD, Goh GKL, Chew RX (2012) Piezoelectrically active hydrothermal $KNbO_3$ thin films. CrystEngComm 14:421–427

[45] Shiraishi T, Kaneko N, Kurosawa M, Uchida H, Hirayama T, Funakubo H (2014) Effects of heat treatment on electrical and electromechanical properties of hydrothermally synthesized epitaxial $(K_{0.51}Na_{0.49})$NbO3 films. Jpn J Appl Phys 53:05FE02

[46] Shiraishi T, Ishikawa M, Uchida H, Kiguchi T, Kurosawa MK, Funakubo H, Konno TJ (2017) Characterization of (111)-oriented epitaxial $(K_{0.5}Na_{0.5})$NbO3 thick films deposited by hydrothermal method. Jpn J Appl Phys 56:10PF04

[47] Shiraishi T, Einishi H, Yasui S et al (2013) Composition dependency of crystal structure, electrical and piezoelectric properties for hydrothermally-synthesized 3 μm-thickness $(K_xNa_{1-x})NbO_3$ films. J Ceram Soc Jpn 121:627–631

[48] Zhou HM, Yi DQ, Zhang Y, Zheng SL (2005) The dissolution behavior of Nb_2O_5, Ta_2O_5 and their mixture in highly concentrated KOH solution. Hydrometallurgy 80:126–131

[49] Grigoriev A, Yang C, Azad MM, Causey O, Walko DA, Tinberg DS, McKinstry ST (2015) Piezoelectric and dielectric properties of Pb(Zr, Ti)$_O$3 ferroelectric bilayers. Phys Rev B 91:104106

[50] Lupi E, Ghosh A, Saremi S, Hsu SL, Pandya S, Velarde G, Fernandez A, Ramesh R, Martin LW (2020) Large polarization and susceptibilities in artificial morphotropic phase boundary $PbZr_{1-x}Ti_xO_3$ superlattices. Adv Electron Mater 6:1901395

[51] Kim DJ, Maria JP, Kingon AI, Streiffer SK (2003) Evaluation of intrinsic and extrinsic contributions to the piezoelectric properties of $Pb(Zr_{1-x}T_x)O_3$ thin films as a function of composition. J Appl Phys 93:5568–5575

[52] Yu Q, Zhu FY, Cheng LQ, Wang K, Lia JF (2014) Determination of crystallographic orientation of lead-free piezoelectric (K, Na)Nb$_O$3 epitaxial thin films grown on SrTi$_O$3 (100) surfaces. Appl Phys Lett 104:102902

[53] Megaw HD (1968) The thermal expansion of interatomic bonds, illustrated by experimental evidence from certain niobates. Acta Cryst A24:589–604

[54] Wang KP, Wang JY, Zhang HJ, Yu YG, Wu J, Gao WL, Boughton RI (2008) Thermal properties of cubic KTa_{1-x}-Nb_xO_3 crystals. J Appl Phys 103:033513

[55] Shibata K, Suenaga K, Nomoto A, Mishima T (2009) Curie temperature, biaxial elastic modulus, and thermal expansion coefficient of (K, Na)Nb$_O$3 piezoelectric thin films. Jpn J Appl Phys 48:121408

[56] Herdier R, Detalle M, Jenkins D, Remiens D, Grebille D, Bouregba R (2008) The properties of epitaxial PMNT thin

films grown on $SrTiO_3$ substrates. J Cryst Growth 311:123–127

[57] Kim DM, Eom CB, Nagarajan V, Ouyang J, Ramesh R, Vaithyanathan V, Schlom DG (2006) Thickness dependence of structural and piezoelectric properties of epitaxial $Pb(Zr_{0.52}Ti_{0.48})O_3$ films on Si and $SrTiO_3$ substrates. Appl Phys Lett 88:142904

[58] Han G, Ryu J, Yoon WH, Choi JJ, Hahn BD, Park DS (2011) Effect of film thickness on the piezoelectric properties of lead zirconate titanate thick films fabricated by aerosol deposition. J Am Ceram Soc 94:1509–1513

[59] Wang L, Ren W, Yao K, Shi P, Wu X, Yao X (2012) Effects of thickness on structures and electrical properties of $K_{0.5}$-$Na_{0.5}NbO_3$ thick films derived from polyvinylpyrrolidone-modified chemical solution. Ceram Int 38S:S291–S294